OPEN ACCESS
JOURNAL OF ADVANCED DIELECTRICS
Vol. 13, No. 2 (2023) 2250023 (11 pages)
© The Author(s)
DOI: 10.1142/S2010135X22500230

Ferroelectric solid solutions with perovskite- and columbite-type components: From structures formation to domain and hysteresis phenomena

M. O. Moysa[*,‖], V. Yu. Topolov[†], K. P. Andryushin[*], A. V. Nagaenko[‡], L. A. Shilkina[*], M. V. Il'ina[§], O. I. Soboleva[¶], S. Sahoo[*] and L. A. Reznichenko[*]

[*]*Research Institute of Physics, Southern Federal University, 194 Stachki Avenue Rostov-on-Don 344090, Russia*

[†]*Department of Physics, Southern Federal University, 5 Zorge Street Rostov-on-Don 344090, Russia*

[‡]*Institute of High Technologies and Piezotechnics, Southern Federal University 10 Milchakov Street, Rostov-on-Don 344090, Russia*

[§]*Institute of Nanotechnologies, Electronics and Equipment Engineering Southern Federal University, Taganrog 347922, Russia*

[¶]*Research Laboratory of Functional Nanomaterials Technology Southern Federal University, Taganrog 347922, Russia*

[‖]moysa@sfedu.ru

Received 22 August 2022; Revised 19 October 2022; Accepted 8 November 2022; Published 3 December 2022

The paper reports results on the complex study on ferroelectric ceramics that represent solid solutions containing components with a perovskite-type or columbite-type structure. Solid solutions of a three-component $(1-x-y)NaNbO_3$–$xKNbO_3$–$yCdNb_2O_6$ system are manufactured at $x = 0.05$–0.20 and $y = 0.10$. Domain structures in ceramic grains are studied. The consistency between experimental and calculated results is examined for coexisting phases split into non-180° domains (mechanical twins) in the solid solution with $x = 0.15$. A correlation between the internal structure (crystal, domain, granular, and defect) and fundamental electromechanical and polarization properties is stated for the studied three-component solid solutions.

Keywords: Ferroelectric materials; KNN; elastic matching; crystal structure; domain structure; electrophysical properties.

1. Introduction

Crystallographic (domain/polarization) engineering[1–5] has been widespread in ferroelectric materials for the last 20 years, and is concerned with the dependences of physical properties on the state of crystal and/or domain structure in the search for promising functional media. This research direction promoted the formation of a new strategy for the materials' design and element base of electronic devices. This element base comprises the following aspects:

(i) ferroelectric ceramic materials that contain a perovskite PZT ($Pb(Ti,Zr)O_3$) system dominating in the world market,[5–10]
(ii) lead-free, environmentallyfriendly[11–19] n-component solid solutions ($n > 2$) that contain niobates of alkali and alkaline earth metals from various structural families (pseudoilmenite, columbite, layered perovskite-like, etc.),[20,21] and
(iii) multiferroic materials that combine both ferroelectric and ferromagnetic (or antiferromagnetic) properties.[22–25]

In contrast to the PZT system that is of fundamental importance and value in the technological and material-science sense and is an object of studies,[26,27] an insufficiency and inconsistency of information on the properties of complex lead-free solid solutions (including those with nonisostructural components) limit the practical use of these materials.

In the work,[28] optimal conditions were found for the preparation of solid solutions of the $(1-x-y)NaNbO_3$–$xKNbO_3$–$yCdNb_2O_6$ system in the ceramic version. A phase diagram of the state of a fragment of this system adjacent to NaNbO3 was built. For this system, the "composition–structure–properties" links were determined. Based on the obtained results, a complex sequence of diverse (polymorphic and morphotropic) phase transitions was stated, and nonmonotonic molar-concentration dependences of the electrophysical parameters were revealed at room temperature. These dependences correspond to the logic of changes in the electrophysical parameters in systems with morphotropic phase boundaries and intraphase transitions. By means of dielectric spectroscopy, regions of stability of solid solutions

‖Corresponding author.

This is an Open Access article published by World Scientific Publishing Company. It is distributed under the terms of the Creative Commons Attribution 4.0 (CC BY) License which permits use, distribution and reproduction in any medium, provided the original work is properly cited.

with a different nature of the manifestation of ferroelectric properties were found. These properties indicated the presence of diffuse phase transitions or ferroelectric-relaxor behavior. An analysis of macroscopic responses in the system indicated four groups of solid solutions with the promising parameters as follows:

(i) Materials with the dielectric permittivity at constant mechanical stress $2000 < \varepsilon^{\sigma}_{33}/\varepsilon_0 < 2250$ are suitable for applications in a midrange,
(ii) Materials with $\varepsilon^{\sigma}_{33}/\varepsilon_0 < 750$ and a planar electromechanical coupling factor ~ 0.40 are suitable for applications in microwave devices,
(iii) Materials with $\varepsilon^{\sigma}_{33}/\varepsilon_0$ = 500–700 and a piezoelectric voltage coefficient $g_{33} \approx 30$ mV·m/N are suitable for high-sensitive accelerometers and ultrasound defectoscopes, and
(iv) Materials with the mechanical quality factor $Q_m \approx 1000$ and $K_p \approx 0.20$ are suitable as active elements of devices that operate in power modes.

In fact, the aforementioned properties and their dependences on external field are closely associated with the ferroelectric domain structure in the studied solid solutions.[29,30] In this context, it is relevant to establish a correlation between the domain structure and macroresponses of these materials. To solve this problem, it is important to consider models for describing the physical processes in ferroelectric ceramics.

In this paper, we highlight the physical mechanisms of forming the internal (crystal, domain, and granular) structure in ceramic $(1–x–y)NaNbO_3–xKNbO_3–yCdNb_2O_6$ with x = 0.05–0.20 and $y = 0.10$, wherein the perovskite-type ((Na,K)-NbO_3) and columbite-type ($CdNb_2O_6$) compounds are present. We also study the effect of the internal structure on the physical properties of the solid solutions for the purpose of subsequent control of their parameters by means of external influences such as temperature T, DC electric field E, amplitude E_m, and frequency f of the AC electric field.

2. Objects and Methods to Manufacture and Study Samples

2.1. *Objects of the study and manufacturing*

In this paper, we study solid solutions of the $(1–x–y)$-$NaNbO_3–xKNbO_3–yCdNb_2O_6$ system at x = 0.05–0.20, y = 0.10 and $\Delta x = 0.05$. The samples were obtained by a two-stage solid-phase synthesis and sintered by a conventional ceramic technology (temperature $T_{\text{synth.1}} = 1220$ K, time τ_1 = 5 h, $T_{\text{csynth.2}} = 1240$ K, $\tau_2 = 10$ h, $T_{\text{sintering}}$ = (1180–1190) K, depending on the composition, and $\tau_{\text{sintering}} = 2$ h). Sintered ceramic blanks were a subject of a mechanical treatment (cutting on a plane, grinding on flat surfaces and ends) for further manufacturing of samples involved in measurements. These samples were disk-shaped with a diameter of 10 mm and thickness of 1 mm. Before metallization, the samples were calcined at $T_{\text{calc}} = 770$ K for 0.5 h to remove organic residues and degreasing surfaces in order to increase an adhesion of metal coating to a ceramic. The samples were electroded by double burning of silver-containing paste at $T = 1070$ K for 0.5 h.

Poling of the samples was carried out in a chamber with polyethylene siloxane liquid at $T_{\text{pol}} \approx 413$ K. Heating up to T_{pol} was carried out according to the linear law during 0.5 h. Hereby, an increase of the electric field was performed from $E = 0$ to $E = 3$ kV/mm. Under these conditions, the samples were kept for 25 min, and hereafter the samples were cooled under the electric field to $T \approx 298$ K.

2.2. *Methods to study samples*

X-ray structural studies were carried out at room temperature by using a DRON-3 diffractometer (filtered CuKα radiation, the Bragg–Brentano focusing scheme). Bulk and crushed ceramic objects were studied to exclude the effect of surface, stress and textures when manufacturing the ceramic samples. An evaluation of structural parameters was performed in terms of known approaches.[31]

A domain structure was studied by means of the piezoresponse force microscopy (PFM), within a potential of the probe nanolaboratory NTEGRA (NT-MDT SI, Russia). A conductive cantilever HA_NC/Pt was used as a probe, and this cantilever was characterized by a force constant of 12 N/m and resonance frequency of 235 kHz. Scanning was carried out at the probe oscillation frequency of 5 kHz and bias voltage of 10 V. The difference in surface relief was 300 nm.

To study a microstructure of sample cleavages, we used a scanning electron microscope JSM-6390L (JEOL, Japan) with a system of microanalyzers from Oxford Instruments, UK. Hereby, the microscope resolution achieved 1.2 nm at an accelerating voltage of 30 kV (image in secondary electrons), limits of the accelerating voltage was from 0.5 to 30 kV, the magnification range was from ×5 to ×300,000, and the beam current was up to 200 nA.

Curves of the unipolar strain (S_{33}) induced by a DC electric field $\boldsymbol{E}(0; 0; E)$ were obtained on poled samples by means of using a measuring stand, including a MICRON-02 gage block tester and an Agilent 34420 A nanovoltmeter/microohmmeter. A $S_{33}(E)$ dependence was approximated with a polynomial, by using the least squares method. A criterion for the quality of the approximation was the minimum value of the standard deviation r. The piezoelectric strain coefficient d_{33} was found by using the formula $d_{33} = dS_{33}/dE$, where "d" in the right part denotes the derivative symbol.

P–E loops of the dielectric hysteresis were studied by means of the Sawyer–Tower method[32,33] at the frequency of the electric field $f = 50$ Hz and temperatures T = 290–430 K. Hereby, the spontaneous (P_s), remanent (P_r) polarizations as well as coercive field (E_c) were determined. A narrow temperature range is due to using polyethylene siloxane oil

as an insulator in a measuring cell, and a boiling point of this oil was near $T = 480$ K. To eliminate the effect of hydrolysis, the ceramic samples were preliminarily annealed at $T = 670$ K.

An analysis of the coexisting ferroelectric phases split into non-180° domain (or twin) structures was carried out within the framework of a crystallographic algorithm put forward by Metrat[34] for the first time. As is known, this algorithm is effectively applied[35] to interpret specifics of phase coexistence in ferroelectrics. Hereby, the coexisting polydomain phases are characterized by distortion matrices $\|M_{ij}\|$ and $\|N_{ij}\|$ which are 3 × 3 matrices. These matrices depend on unit-cell parameters, orientations of crystallographic axes and volume fractions of domain types in the coexisting phases, and on angles of mutual rotations of crystallographic axes of adjacent non-180° domains.[36]

$$\begin{cases} \det\left\|D_{ij}\right\| = 0; \\ \left(D'_{ij}\right)^2 \geq 0, \end{cases} \tag{1}$$

where

$$D_{ij} = \sum_{k=1}^{3} (N_{ik}N_{jk} - M_{ik}M_{jk}). \tag{2}$$

In Eqs. (1) $(D_{ij}')^2 = D_{ij}^2 - D_{ii}D_{jj}$, and N_{ik} and M_{ik} from Eq. (2) are matrix elements from the distortion matrices $\|M_{ij}\|$ and $\|N_{ij}\|$, respectively. Conditions from Eq. (1) are written on assumption that domain walls in the coexisting phases are stress-free and uncharged, and orientations of the domain walls are determined in accordance with concepts.[36]

3. Results and Discussion

Based on roentgenograms of the studied ceramic compositions (Fig. 1), we state that they are characterized by the perovskite-type structure. According to data from work,[28] solid solutions with $x = 0.05$ and 0.10 belong to the tetragonal region of the phase diagram of the $(1-x-y)NaNbO_3$–$xKNbO_3$–$yCdNb_2O_6$ system. Solid solutions with $x = 0.15$ and 0.20 are in the heterogeneous region wherein impurity compounds with the general chemical formula $K_mNb_nO_p$ are present side by side with perovskite-type solid solutions. It is seen from Fig. 1 that a relative intensity of strong peaks of impurity compounds does not exceed 5–7%. Solid solutions with $x = 0.15$ and 0.20 represent mixtures of two phases, namely, tetragonal and orthorhombic with a reduced monoclinic unit cell. A coexistence of several phases with different symmetries and similar cell parameters leads to the superposition of diffraction peaks, and this circumstance makes it difficult to accurately determine the cell parameters of each of the phases. The profile of the (200) diffraction peak of solid solutions with $x = 0.05$, 0.15, and 0.20, which is shown in Fig. 1 on an enlarged scale is characterized by two features as follows. Firstly, this peak is distorted by diffuse scattering at the base. Secondly, the peak indicates a heterogeneity of solid solution even within the same phase. In our opinion, the most homogeneous solid solution is achieved at $x = 0.10$. In Table A.1, we collected results on symmetry and unit-cell parameters of studied solid solutions.

It is stated that solid solutions with $x < 0.15$ are tetragonal, single-phase, and without a superstructure. On further

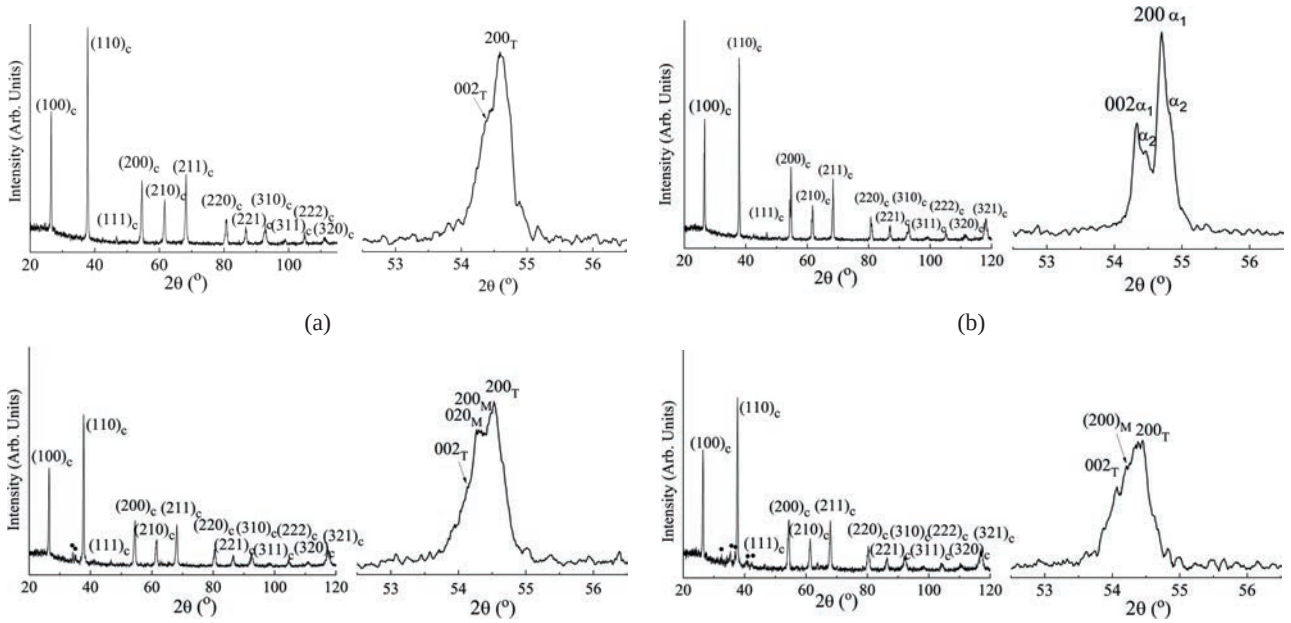

Fig. 1. Roentgenogram of $(1-x-y)NaNbO_3$–$xKNbO_3$–$yCdNb_2O_6$ in the interval of angles $2\theta = (20–120)°$ and a large-scale diffraction reflection $(200)_c$. Indexes of diffraction reflexes refer to the perovskite unit-cell axes: (a) $x = 0.05$, (b) $x = 0.10$, (c) $x = 0.15$, and (d) $x = 0.20$. Dots are used to mark lines of impurity phases.

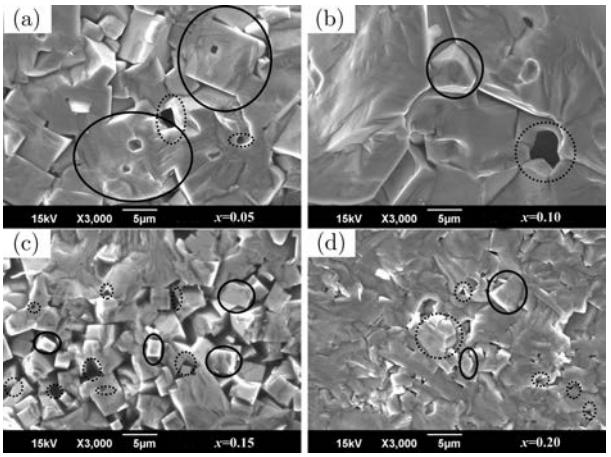

Fig. 2. Fragments of the microstructure of $(1-x-y)NaNbO_3$–$xKNbO_3$–$yCdNb_2O_6$ ceramics with $y = 0.10$ and $x = 0.05$–0.20 (according to the data in Ref. 28).

increasing the molar concentration, at $x \geq 0.15$, heterophase regions with tetragonal and monoclinic phases are detected. Recrystallization phase transitions that occur against a background of such phase transitions lead to a formation of an original granular landscape (Fig. 2) that clearly reacts to all changes in the crystal structure of solid solutions.

The main feature of all the studied solid solution compositions is the formation of idiomorphic grains of a regular geometric shape. The so-called plate-like grains are characteristic of structures that contain liquid phases.[28] In our case, sources of liquid phases can be Na_2CO_3 with the melting temperature of 1126 K, K_2CO_3 with the melting temperature of 1164 K, KOH with the melting temperature of 677 K (i.e., unreacted components and products of their hydrolysis), as well as fusible eutectics in niobate batches ($NaNbO_3$ with the melting temperature 1260 K and $KNbO_3$ with the melting temperature 1118 K), and fusible, fairly reactive fluorides (products of the interaction of fluorine impurity in the main initial component, Nb_2O_5, that actively interacts with basis solid solutions).

From Fig. 2, the refinement of the grain landscape is observed when increasing the molar-concentration x of $KNbO_3$.[28] At $x = 0.15$ (coexistence of monoclinic and tetragonal phases), a sharp (4–5 times) decrease in grain size (highlighted with a solid line) is observed; intragranular porosity (highlighted with a dashed line) being typical of solid solutions with $x = 0.05$ and 0.10, and a structure compaction. The aforementioned effects are most likely concerned with a saturation of the system with the liquid phase that surrounds grain boundaries and, to a large degree, hinders processes of diffusion and mass transfer. These factors lead to the refinement of the microstructure of the ceramic samples.

The solid solution with the composition $0.75NaNbO_3$–$0.15KNbO_3$–$0.10CdNb_2O_6$ belongs to the morphotropic phase boundary and contains monoclinic and tetragonal phases with similar perovskite unit-cell parameters, see Table A.1. When describing the coexisting monoclinic and tetragonal phases in heterophase compositions studied by us, it is assumed that

(i) the monoclinic phase is split into the non-180° domains that are separated by planar domain walls oriented parallel to planes of the {100} type in the perovskite unit cell, and
(ii) the tetragonal phase is split into the 90° domains, and domain walls between these domains are parallel to planes of the {110} type in the perovskite unit cell.[35]

Based on concepts,[35,36] we assume that the aforementioned domain walls are stress-free and electrically noncharged. An example of the mutual arrangement of domains (mechanical twins) in the coexisting ferroelectric phases is graphically shown in Fig. 3. Hereby, it is assumed that orientations of domains of the monoclinic phase (Fig. 3(a)) slightly differ from the domain orientations in the rhombohedral phase of PZT-type solid solutions.[35]

Volume fractions of the two 90° domain types in the tetragonal phase equal q and $1-q$, respectively, see Figs. 3(b) and 3(c). Volume fractions of the four 71° (109°) domain types in the monoclinic phase are written in terms of parameters x_R and y_R, see Fig. 3(a). In the tetragonal phase, we consider two domain types and do not take into account domains of the type 6 with the spontaneous polarization vector oriented parallel to the OX_2 axis. The distortion matrix of the polydomain monoclinic phase is written by analogy with the distortion matrix of the rhombohedral phase[35] as follows:

$$\|M_{ij}\| = \begin{pmatrix} \mu_a & \mu(2y_R-1) & \mu(2x_R-1)(2y_R-1) \\ \mu(2y_R-1) & \mu_a & \mu(2x_R-1) \\ \mu(2x_R-1)(2y_R-1) & \mu(2x_R-1) & \mu_a \end{pmatrix}. \quad (3)$$

The distortion matrix of the polydomain tetragonal phase can be represented as

$$\|N_{ij}^{5-6}\| = q\begin{pmatrix} \varepsilon_a & 0 & 0 \\ 0 & \varepsilon_a & 0 \\ 0 & 0 & \varepsilon_c \end{pmatrix} + (1-q)\begin{pmatrix} 1 & 0 & 0 \\ 0 & \cos\varphi_t & -\sin\varphi_t \\ 0 & \sin\varphi_t & \cos\varphi_t \end{pmatrix}\begin{pmatrix} \varepsilon_a & 0 & 0 \\ 0 & \varepsilon_c & 0 \\ 0 & 0 & \varepsilon_a \end{pmatrix}, \quad (4)$$

for domain types 5 and 6 in Fig. 3(b), or as

$$\|N_{ij}^{5-7}\| = q\begin{pmatrix} \varepsilon_c & 0 & 0 \\ 0 & \varepsilon_a & 0 \\ 0 & 0 & \varepsilon_a \end{pmatrix} + (1-q)\begin{pmatrix} \cos\varphi_t & 0 & -\sin\varphi_t \\ 0 & 1 & 0 \\ \sin\varphi_t & 0 & \cos\varphi_t \end{pmatrix}\begin{pmatrix} \varepsilon_a & 0 & 0 \\ 0 & \varepsilon_a & 0 \\ 0 & 0 & \varepsilon_c \end{pmatrix}, \quad (5)$$

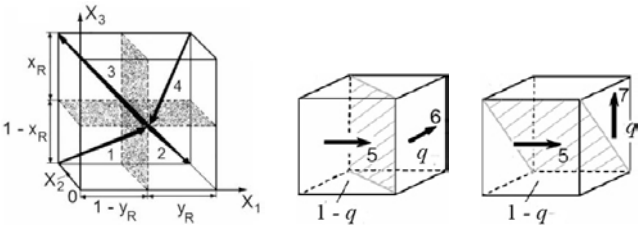

Fig. 3. Orientations of spontaneous polarization vectors of non-180° domains in the monoclinic (a) and tetragonal (b, c) phases (reprinted from monograph by Topolov,[35] with permission from Springer).

for domain types 5 and 7 in Fig. 3(c). Equations (3)–(5) are written in terms of distortions of the perovskite unit cell $\mu_a = a_M \cos(\omega_M)/a_C$, $\mu = a_M \sin(\omega_M)/a_C$, $\varepsilon_a = a_{\text{Tetr.}}/a_C$, and $\varepsilon_c = c_{\text{Tetr.}}/a_C$, where a_C is the unit-cell parameter in the cubic paraelectric phase, relative to which distortions of all the domain types in the coexisting phases are considered. The angle $\varphi_t = \arccos(2\varepsilon_a\varepsilon_c/(\varepsilon_a^2 + \varepsilon_c^2))$ from Eqs. (4) and (5) is used to describe a rotation of the crystallographic axes of the adjacent 90° domains in the tetragonal phase. Thus, the unit-cell distortions depend on the unit-cell parameters of the monoclinic (a_M and ω_M) and tetragonal ($a_{\text{Tetr.}}$ and $c_{\text{Tetr.}}$) phases, and a_C plays the role of a constant and does not influence our further calculation results. Matrix elements D_{ij} from Eq. (2) are to be found by taking into account the distortion matrices from Eqs. (3) and (4) (see the domain arrangement in Figs. 3(a) and 3(b)) or from Eqs. (3) and (5) (see the domain arrangement in Figs. 3(a) and 3(c)).

Two roots q_i, that obey conditions (1) and take values from the [0; 1] range, are optimal volume fractions of the domain type denoted with "q" in Figs. 3(b) or 3(c). Now, we find the optimal volume fractions qi of the 90° domains in the tetragonal phase that coexists with the polydomain monoclinic phase at $x = 0.15$. The optimal volume fractions q_i mean that conditions (1) hold at the planar interfaces between the coexisting phases and there is no excess elastic energy in heterophase regions. In the monoclinic phase, both the x_R и y_R parameters from Fig. 3(a) can be varied from 0 to 1, and validity of conditions (1) is examined at x_R = const. and y_R = const. Values of q_i are found for the tetragonal phase that is split into the 90° domains according to one of two versions, types 5 and 6 (see Fig. 3(b)), or types 5 and 7 (Fig. 3(c)).

It is found that at $x_R = 1$, 0.9, 0.8, 0.2, and 0.1, and $y_R = 1$, 0.9, 0.8, 0.2, and 0.1, there are regions of forbidden volume fractions q in the tetragonal phase split into domains of types 5 and 7. This means that conditions (1) are not valid in such heterophase structures. In the case of the presence of domains of types 5 and 6 in the same tetragonal phase, as x_R changes from 1 to 0.5 or from 0.1 to 0.5, we observe some patterns of changes in the width of the region of the forbidden volume fractions q. For instance, at $x_R = 1$, 0.9, and 0.1, one can find the forbidden volume fractions q at $y_R = 0.1$, (0.3–0.7), and (0.9–1); at $x_R = 0.8$ and 0.2, the forbidden volume fractions q are observed in narrower ranges of y_R = (0.3–0.7) and at $y_R \approx 1$. At $x_R = 0.7$, 0.6, 0.4, and 0.3, we observe the similar behavior of q, and the region of the forbidden volume fractions becomes narrower, i.e., y_R = (0.3–0.7).[37] In other cases, the presence of the region of the forbidden volume fractions is not observed.

No obvious tendency to a monodomainization of the tetragonal phase with domains of types 5 and 7 was found. In the case of the tetragonal phase with domains of types 5 and 6, the tendency to the monodomainization is noted at $x_R = 0.8$ and 0.2, and $y_R = 0.1$ and 0.9.

It is stated that the volume fraction q of domain of type 5 in the polydomain tetragonal phase shown in Fig. 3(c) undergoes changes depending on values of x_R и y_R in the monoclinic phase. For instance, at $x_R = 0.3$ or 0.7, we have q_1 = 0.22, at $x_R = 0.4$ or 0.6, we have q_1 = 0.19–0.37, and at x_R = 0.5, we have 0.42.

Volume fractions of domains of types 5 and 6 are linked by the ratio $(1-q_1)/q_1 = 0.25/0.75$ at x_R = (0.2–0.3), (0.7–0.8), y_R = (0.1–0.2), (0.8–0.9). At $x_R = 0.3$ and 0.7, and $y_R = 0.2$ and 0.8, the ratio $(1-q_1)/q_1 = 0.35/0.65$ holds. At $x_R = 0.1$ and 0.9, and $y_R = 0.2$ and 0.8, the ratio $q_2/q_1 = 0.12/0.88$ is achieved, and at $x_R = 0.5$ and y_R = (0.1–1) the ratio $(1-q_1)/q_1$ equals 0.42/0.58. Thus, we observe a tendency to an equalization of the volume fractions of the 90° domain types in the tetragonal phase.

Figure 4 shows dependences of the optimal volume fractions of domains of the type 5 (two solutions, q_1 and q_2) on y_R at $x_R = 0.5$ and dependences of the optimal volume fractions of domains of the type 5 on y_R, where y_R = 0.1–1.

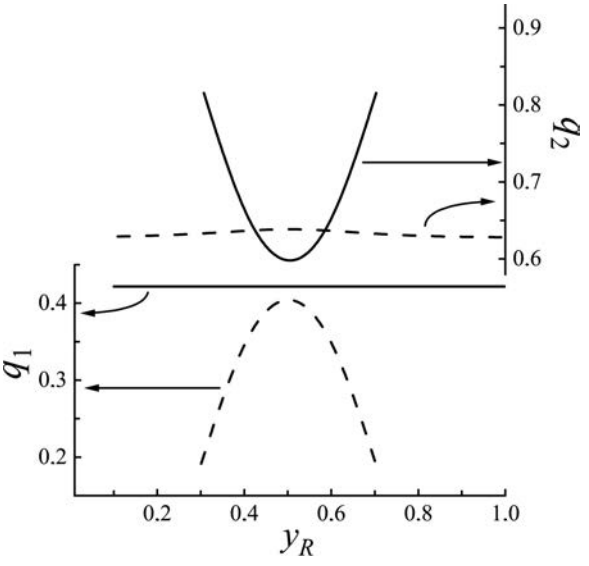

Fig. 4. Calculated dependences of optimal volume fraction q_i (i = 1 and 2) of 90° domains in the tetragonal phase on the concentration parameter y_R of domains in the monoclinic phase at x_R = 0.5 (solid line) and $x_R = 0.4$ (dotted line) in $0.75NaNbO_3$–$0.15KNbO_3$–$0.10CdNb_2O_6$ at room temperature.

At $x_R = 0.8$ and $y_R = 0.03$ (or $y_R = 0.98$), complete stress relief is achieved at the tetragonal-monoclinic interfaces, and the optimal volume fraction q_1 of the 90° domains of the type 5 in the tetragonal phase (see Fig. 3(b)) becomes minimal. According to our evaluations, in this case the value of $q_1 = 0.0032$ is achieved. Conditions $x_R = 0.8$ and $y_R = 0.03$ (or $y_R = 0.98$) suggest that in the monoclinic phase (see Fig. 3(a)) almost two domain types can be taken into account when analyzing stress–relief conditions. The presence of two domain types in the monoclinic phase leads to a simplification of the distortion matrix $\|M_{ij}\|$ from Eq. (3). The large difference between the optimal volume fractions of the 90° domains $q_1 = 0.0032$ and $q_2 = 0.9968$ indicates that the tetragonal phase is monodomain in the case when the monoclinic phase is represented by almost two domain types. In fact, a decrease of the number of the non-180° domain types in a heterophase sample contributes to a simpler picture of domain-orientation effects that influence the formation of piezoelectric and other properties.

Studies on the domain structure and piezoelectric properties enable us to note that the poled ceramic samples demonstrate significant longitudinal and transverse piezoelectric responses. An image contrast (Fig. 5) suggests that the longitudinal piezoelectric response is more than 10 times stronger in comparison to the transverse piezoelectric response.

The domains are located on the surface in a chaotic manner: most of the domains have a predominantly longitudinal piezoelectric response (see dark regions in Fig. 5(a)) with a slight transverse piezoelectric response. Smaller domains with predominantly transverse piezoelectric response are also present in the studied samples (see dark regions in Fig. 5(b)).

The contrast on the signal of phase 1 (the orientation of domains is perpendicular to the surface, see Fig. 5(a)) is almost nonvisible. This means that the vectors of the longitudinal polarization of these domains are mainly oriented in one direction. Visible small dark areas stand out from the overall field, and these areas are presumably regions of the monoclinic phase with non-180° domains. In this case, parallels

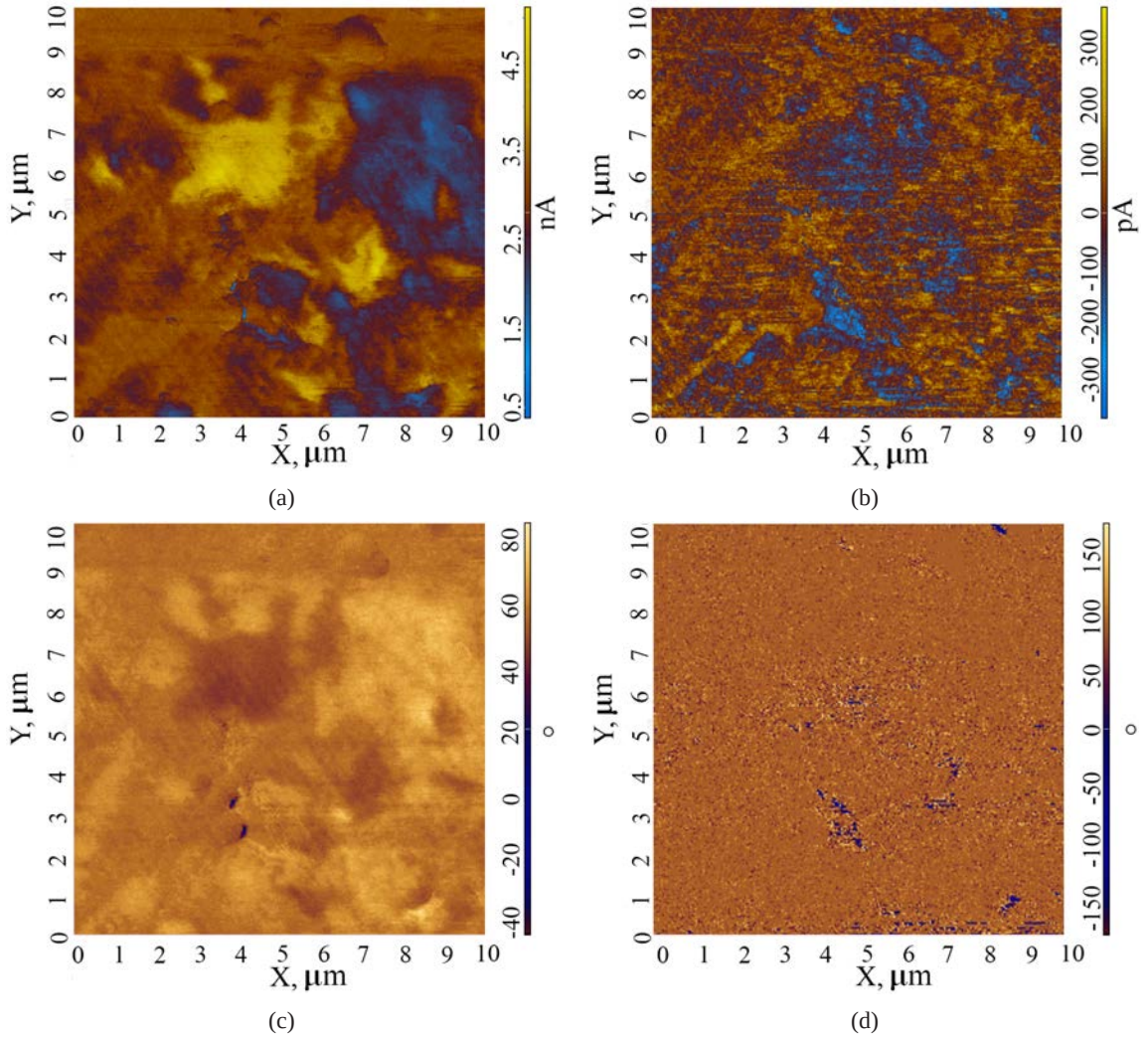

Fig. 5. Characteristics of domain structure and piezoresponse of $0.75NaNbO_3$–$0.15KNbO_3$–$0.10CdNb_2O_6$ with $y = 0.10$ and $x = 0.15$ at $T = 300$ K: (a), (c) amplitude and phase of longitudinal piezoresponse, (b), (d) amplitude and phase of transverse piezoresponse.

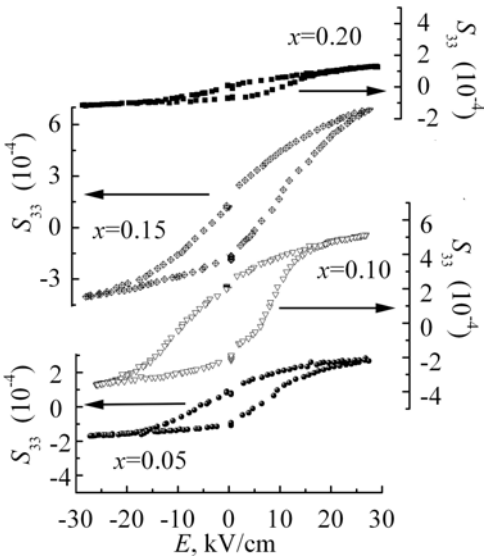

Fig. 6. $S_{33}(E)$ loops of ceramic $(1-x-y)NaNbO_3-xKNbO_3-yCdNb_2O_6$ at $y = 0.10$, $x = 0.05$–0.20, and $T = 300$ K.

can be drawn that the tetragonal phase tends to a single-domain state, since the longitudinal polarization vector is predominantly oriented in one direction. The contrasting regions of the phase 2 signal (Fig. 5(d)) indicate that the transverse polarization vector in the regions with a tone of ~ −100° has the opposite direction relative to the rest of the region with a tone of ~125°.

An evolution of electromechanical hysteresis loops depending on the molar-concentration x of $KNbO_3$ is shown in Fig. 6. It is revealed in the studied ceramic samples that the electric field dependence of the longitudinal strain $S_{33}(E)$ in the second half-cycle of the loop is located in the third quarter of the "strain–electric field" coordinate system. This behavior remotely resembles a dielectric hysteresis loop of ferroelectrics. From Fig. 6, on increasing the molar-concentration x up to $x = 0.15$, a gradual expansion of the electromechanical hysteresis loop is observed.

However, at $x = 0.20$, a significant narrowing of the loop along the ordinate axis is observed, see Fig. 6. The loop shapes of the studied solid solutions at small molar-concentrations x, may be due to a softness of the crystal structure. Apparently, the further expansion of the loops on increasing x (or with the larger molar concentration of $KNbO_3$) is associated with an increase of a hardness of the structure due to a more pronounced heterogeneity of the studied ceramic samples. It should be noted that the electromechanical hysteresis loop at $x = 0.15$ is characterized by a large tangent slope, see Fig. 6. Moreover, this performance manifests itself even in sufficiently weak fields E. In our opinion, this behavior is facilitated by valid conditions for complete stress relief in the presence of a limited number of domain types, as well as when the morphotropic phases tend to monodomainization.

In Fig. 7, half-cycles of the electromechanical hysteresis loops and strains related to these loops are graphically shown. Based on these data, we evaluated the remanent (S_r), maximal (S_{max}), and delta strains ($\Delta S = S_{33}^{+} - S_{33}^{-}$ at $E = 15.5$ kV/cm). In the molar-concentration range of $0.05 \le x \le 0.10$, a gradual increase in the strain characteristics is observed. At $x = 0.15$ (impurity fraction < 5%), in the heterophase region, the formation of extremum points of the aforementioned strain

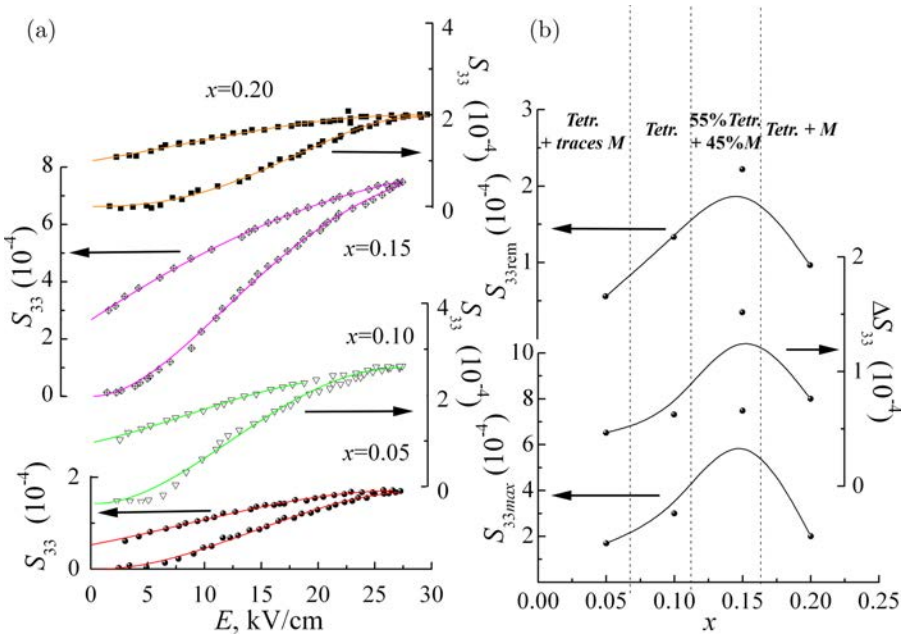

Fig. 7. Half-cycles of $S_{33}(E)$ loops (a) and compositional dependence of the remanent (S_r), maximal (S_{max}), and delta strains (ΔS) (b) in the $(1-x-y)NaNbO_3-xKNbO_3-yCdNb_2O_6$ system at $y = 0.10$, $x = 0.05$–0.20, $T = 300$ K, and $E \approx$ (0–30) kV/cm.

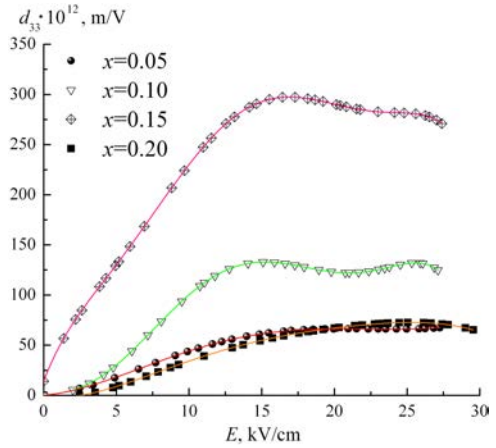

Fig. 8. $d_{33}(E)$ curves of $(1–x–y)NaNbO_3–xKNbO_3–yCdNb_2O_6$ at $y = 0.10$ and $x = 0.05–0.20$.

parameters is revealed, and at $x > 0.15$, a sharp decrease of these parameters is observed (Fig. 7(b)).

The $d_{33}(E)$ curves were obtained from the ascending branch of the loop of the electromechanical hysteresis at $0.05 \le x \le 0.20$ (Fig. 8). It is stated that in solid solutions with $x = 0.10$ and 0.15, the $d_{33}(E)$ curves are characterized by a sharp increase of d_{33} up to the DC electric field $E \approx 17$ kV/cm, at which the formation of the extremum of $d_{33}(E)$ is observed (Fig. 8).

This correlates with the behavior of the ascending branch of the half-cycle $S_{33}(E)$ (Fig. 7) and with the further decrease of $d_{33}(E)$ by $(1–23)\cdot10^{-12}$ m/V in the range of $E = (17–30)$ kV/cm. This is possibly due to the fact that in the range of $E = (0–17)$ kV/cm, domain-orientation processes prevail in the monoclinic phase, and at $E \approx 17$ kV/cm, domain-orientation processes are additionally involved in the tetragonal phase. We remind the reader that these results are related to solid

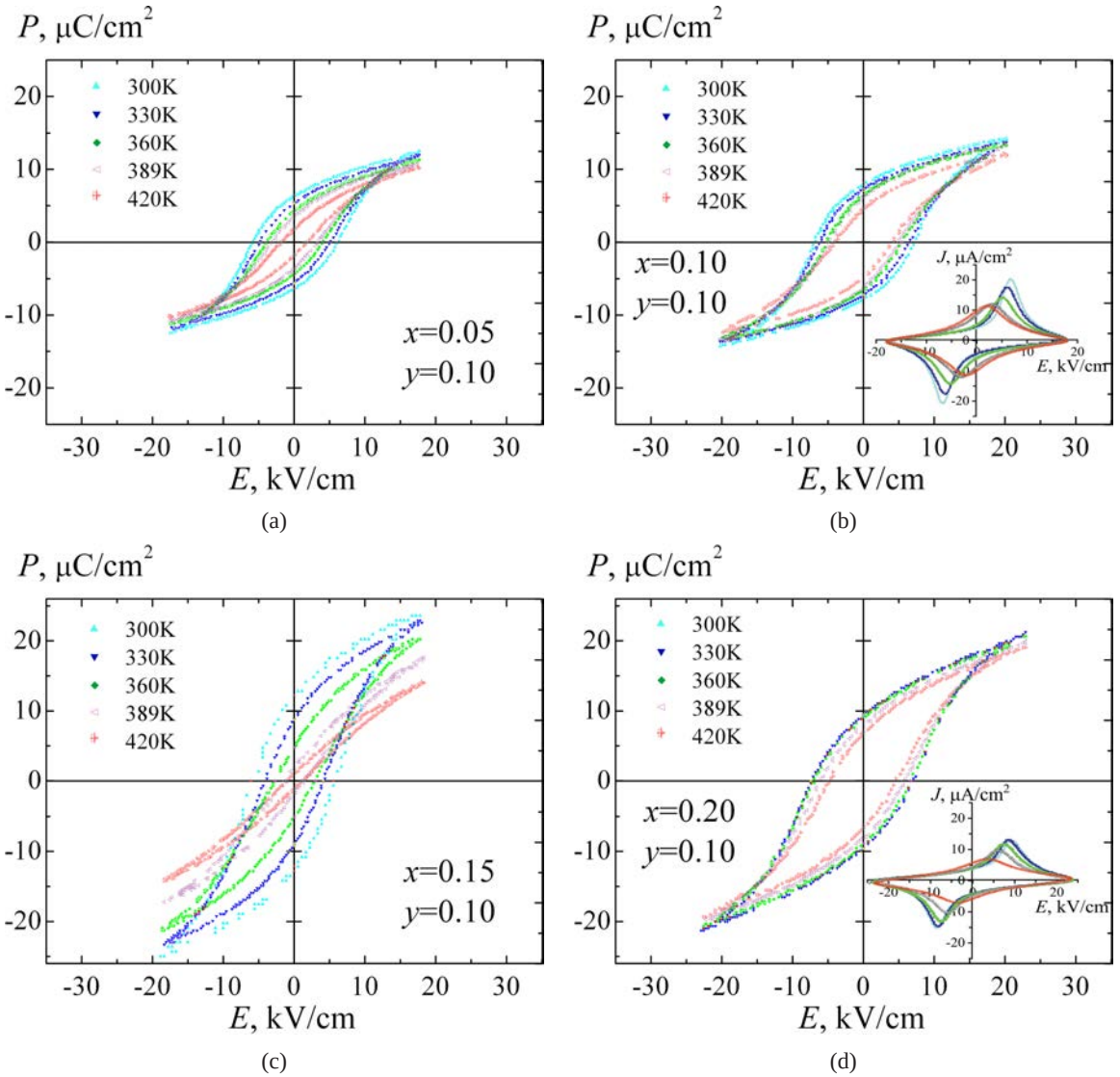

Fig. 9. $P–E$ loops of $(1–x–y)NaNbO_3–xKNbO_3–yCdNb_2O_6$ at $y = 0.10$, $x = 0.05–0.20$ (a–d), $T = (300–420)$ K, and $\Delta T = 30$ K.

solution with $x = 0.15$ for which an approximate equality of volume fractions of the tetragonal and monoclinic phases is known (see Table A.1). It should also be noted that the $d_{33}(E)$ dependence at $x = 0.10$ has two extremum points, namely, a maximum at $E \approx 16$ kV/cm (as noted earlier) and a minimum at $E \approx 20$ kV/cm. At molar-concentrations $x = 0.05$ and 0.20, the $d_{33}(E)$ dependence has no extremum points and is increasing up to $E \approx 17.5$ kV/cm. At larger E values, the plateau-like character of the $d_{33}(E)$ curve is observed, see Fig. 8.

In Fig. 9, an evolution of the dielectric hysteresis loops (P–E loops) is shown depending on temperature T ranging from 300 to 420 K, at various molar-concentrations x of $KNbO_3$. It is revealed that in solid solutions at $0.05 \le x \le 0.10$ (Figs. 9(a) and 9(b)) and $x = 0.20$ (Fig. 9(d)), the saturated P–E loops are formed at the electric field E = (14–17) kV/cm in the whole aforementioned temperature range. At x = 0.15, the nonsaturated P–E loops are observed (Fig. 9(c)) at T = (300–340) K and $E \approx 14$ kV/cm. A further increase of temperature leads to the formation of the saturated P–E loops. Inserts in graphs in Figs. 9(b) and 9(d) show current density loops at $x = 0.10$ and 0.20, and T = (300–420) K.

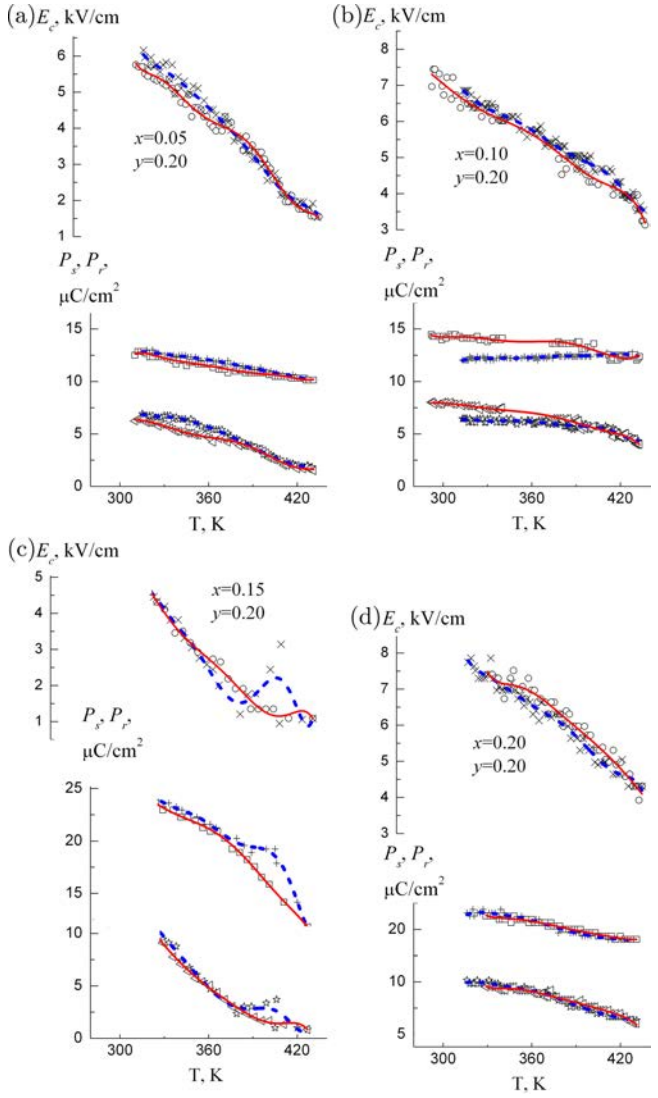

Fig. 10. $P_s(T)$, $P_r(T)$, and $E_c(T)$ dependences of $(1-x-y)NaNbO_3$–$xKNbO_3$–$yCdNb_2O_6$ with x = 0.05–0.20 (a–d) and $y = 0.10$.

Based on the results of the study on the P–E loops, we have built temperature dependences of P_s, P_r, and E_c (Fig. 10) which have been approximated by a second-degree polynomial. In solid solutions with $0.05 \le x \le 0.15$ (Figs. 10(a)–10(c)), a formation of three regions of the temperature dependences of P_s, P_r, and E_c is revealed, and these dependences are characterized by various changes of the slope angle at T = 360 and 405 K. On heating in the range of T = (290–360) K, there is a large decrease of the aforementioned dependences. On heating over T = 360 K, the $P_s(T)$, $P_r(T)$, and $E_c(T)$ dependences undergo minor changes, and a quasi-minimum is formed at T = 405 K. In the range of T = (405–430) K, as one approaches the Curie temperature (445–460) K, the slope angle of the $P_s(T)$, $P_r(T)$, and $E_c(T)$ curves increases significantly. It should be added that the aforementioned anomalies have a restricted effect on the P_s value and are minor in several cases. On heating and cooling within the temperature range of T = (300–380) K, in solid solutions with $0.05 \le x \le 0.10$, a temperature hysteresis is observed, and this is concerned with the temperature behavior of $P_s(T)$, $P_r(T)$, and $E_c(T)$. At $x = 0.15$, the noticeable $P_s(T)$, $P_r(T)$, and $E_c(T)$ dependences are registered in a narrower temperature range, namely, at $T \approx$ (340–430) K. In this temperature range, the polarization decreases to the Curie point T_C = 435 K. The observed anomalies of the parameters at T = 360 and 405 K are likely caused by either a development of defects or by structural instabilities in the studied ceramic samples, and these features need additional X-ray structural studies.

Our research results can be taken into account in the development of piezotechnical devices for various fields of applications concerned with the longitudinal piezoelectric effect, polarization switching, etc.

4. Conclusions

1. Ferroelectric solid solutions of the ternary $(1-x-y)$-$NaNbO_3$–$xKNbO_3$–$yCdNb_2O_6$ system have been obtained at x = 0.05–0.20 and $y = 0.10$. Regions of coexisting morphotropic phases have been revealed. The correspondence between the microstructure and the crystal structure of ceramic samples of this system is shown.
2. Optimal volume fractions of the 90° domains q in the tetragonal phase have been found in coexistence with this and polydomain monoclinic phases in $0.75NaNbO_3$–$0.15KNbO_3$–$0.10CdNb_2O_6$. At $x_R = 0$ and $y_R = 0.19$ or at $x_R = 1$ and $y_R = 0.18$ (i.e., in the presence of two domain types in the monoclinic phase with a large difference between the volume fractions of these domain types), the significant difference between the optimal volume fractions q and $1 - q$ has been stated. This is the indicator of the tendency of the tetragonal phase to monodomainization.

3. Consistency of the results of the experimental study on the domain structure and the results of the analysis of coexisting ferroelectric phases split into the non-180° domains in $0.75NaNbO_3$–$0.15KNbO_3$–$0.10CdNb_2O_6$ has been stated.
4. Rules of the formation of the electromechanical and polarization properties have been determined for the studied solid solutions at various external actions (temperature, DC and AC electric fields).
5. The electromechanical hysteresis loop of solid solution with $x = 0.15$ is characterized by a large slope angle, and this effect is manifested even in weak electric fields. This phenomenon can be explained by taking into account conditions for complete stress relief in the presence of a restricted number of the non-180° domain types and by trends of the ferroelectric phases of $0.75NaNbO_3$–$0.15KNbO_3$–$0.10CdNb_2O_6$ to the monodomainization.
6. At $x = 0.15$, the $d_{33}(E)$ curve is characterized by the sharp increase of d_{33} at the DC electric field E = (0–17) kV/cm, the subsequent formation of extremum points and decrease at E = (17–30) kV/cm. This is accounted for by the feature that at E = (0–17) kV/cm, the domain-orientation processes prevail in the monoclinic phase, and at E = 17 kV/cm, the domain-orientation processes become active in the tetragonal phase.
7. At $x = 0.15$, the nonsaturated state of the P–E loops is observed at T = (300–340) K and E = 14 kV/cm. In solid solutions with $0.05 \le x \le 0.15$, the formation of three regions of the $P_s(T)$, $P_r(T)$ и $E_c(T)$ dependences has been revealed. These dependences are characterized by different changes of their sloop angles near T = 360 K and T = 405 K. The observed anomalies are caused by either defects of structural instabilities in the studied ceramic samples.

Acknowledgments

The study was carried out with the financial support of the Ministry of Science and Higher Education of the Russian Federation (State Task in the Field of Scientific Activity, Scientific Project No. 0852-2020-0032/BAZ0110/20-3-07IF). The authors would like to thank Prof. Dr. C. R. Bowen (University of Bath, UK) for his interest in the research problems and for his careful reading of the paper. M. O. Moysa is grateful to the Southern Federal University Strategic Academic Leadership Program (Priority 2030) for the support of graduate students participating in this study.

Appendix A. Experimental Data on Ferroelectric Phases in Studied Solid Solutions

Table A.1 contains our experimental results on symmetry, unit-cell parameters, and related crystallographic parameters of the phases in $(1–x–y)NaNbO_3$–$xKNbO_3$–$yCdNb_2O_6$ at room temperature.

Table A.1. Symmetry, unit-cell parameters, and related parameters of phases in $(1–x–y)NaNbO_3$–$xKNbO_3$–$yCdNb_2O_6$.

x	y	Symmetry	a, Å	c, Å	$(c/a–1)\cdot10^3$	β, deg	V, Å^3
0.05	0.10	Tetragonal phase	3.911	3.923	3.2		60.0
0.10	0.10	Tetragonal phase	3.902	3.927	6.2		59.8
0.15	0.10	Tetragonal phase (55%) and monoclinic phase (45%)	3.916 3.929	3.948	6.5	90.3	60.6 60.5
0.20	0.10	Tetragonal and monoclinic phases	3.921 3.931	3.946	6.5		60.7

References

[1] S.-E. Park and T. R. Shrout, Ultrahigh strain and piezoelectric behavior in relaxor based ferroelectric single crystals, *J. Appl. Phys.* **82**, 1804 (1997), doi:10.1063/1.365983.

[2] D.-S. Paik, S.-E. Park, S. Wada, S.-F. Liu and T. R. Shrout, E-field induced phase transition in ⟨001⟩-oriented rhombohedral $0.92Pb(Zn_{1/3}Nb_{2/3})O_3$–$0.08PbTiO_3$ crystals, *J. Appl. Phys.* **85**, 1080 (1999), doi:10.1063/1.369252.

[3] S.-E. Park, S. Wada, L. E. Cross and T. R. Shrout, Crystallographically engineered $BaTiO_3$ single crystals for high-performance piezoelectrics, *J. Appl. Phys.* **86**, 2746 (1999), doi:10.1063/1.371120.

[4] R.E. Eitel, S.-E. Park, C.A. Randal and T.R. Shrout, Perovskite materials for high temperature and high performance actuators and transducers, Patent No. US20030031622A1 (2003).

[5] V. Shur, A. Akhmatkhanov, A. Lobov and A. Turygin, Self-assembled domain structures: From micro- to nanoscale, *J. Adv. Dielect.* **5**, 1550015 (2015), doi:10.1142/S2010135X15500150.

[6] A. Tawfik, O.M. Hemeda, A.M.A. Henaish and A.M. Dorgham, High piezoelectric properties of modified nano lead titanate zirconate ceramics, *Mater. Chem. Phys.* **211**, 1 (2018), doi:10.1016/j.matchemphys.2018.01.073.

[7] I.A. Shvetsov, M.A. Lugovaya, M.G. Konstantinova, P.A. Abramov, E.I. Petrova, N.A. Shvetsova and A.N. Rybyanets, Dispersion characteristics of complex electromechanical parameters of porous piezoceramics, *J. Adv. Dielect.* **12**, 2160004 (2022), doi:10.1142/S2010135X21600043.

[8] X. Hu, X. Li, K. Yan, X. Qi, W. Chen and D. Wu, Fabrication of porous PZT ceramics using micro-stereolithography technology, *Ceram. Int.* **47**, 32376 (2021), doi:10.1016/j.ceramint.2021.08.137.

[9] L. Bian, X. Qi, K. Li, J. Fan, Z. Li, E. Sun, B. Yang, S. Dong and W. Cao, High-performance $Pb(Ni_{1/3}Nb_{2/3})O_3$-$PbZrO_3$-$PbTiO_3$ ceramics with the triple point composition, *J. Eur. Ceram. Soc.* **41**, 6983 (2021), doi:10.1016/j.jeurceramsoc.2021.07.034.

[10] T. Feng and M. H. F. Aliabadi, Structural integrity assessment of composites plates with embedded PZT transducers for structural health monitoring, *Materials* **14**, 6148 (2021), doi:10.3390/ma14206148.

[11] S. Zhang, R. Xia, T.R. Shrout, G. Zang and J. Wang, Characterization of lead free $(K_{0.5}Na_{0.5})NbO_3$–$LiSbO_3$ piezoceramic, *Solid State Commun.* **141**, 675 (2007), doi:10.1016/J.SSC.2007.01.007.

[12]H. Wei, H. Wang, Y. Xia, D. Cui, Y. Shi, M. Dong, C. Liu, T. Ding, J. Zhang, Y. Ma, N. Wang, Z. Wang, Y. Sun, R. Wei and Z. Guo, An overview of lead-free piezoelectric materials and devices, *J. Mater. Chem. C* **6**, 12446 (2018), https://doi. org/10.1039/c8tc04515a.

[13]K. Xi, Y. Li, Z. Zheng, L. Zhang, Y. Liu and Y. Mi, Study on phase transitions and temperature stability of (1-x)$K_{0.5}Na_{0.5}NbO_3$-x$Bi(Zn_{0.5}Zr_{0.5})O_3$ lead-free ceramics, *Mater. Chem. Phys.* **250**, 123032 (2020), doi:10.1016/j.matchemphys.2020.123032.

[14]Z. Tan, S. Xie, L. Jiang, J. Xing, Y. Chen, J. Zhu, D. Xiao and Q. Wang, Oxygen octahedron tilting, electrical properties and mechanical behaviors in alkali niobate-based lead-free piezoelectric ceramics, *J. Materiomics* **5**, 372 (2019), doi:10.1016/j.jmat.2019.02.001.

[15]J.G. Wu, *Advances in Lead-Free Piezoelectric Materials* (Springer, Singapore, 2018).

[16]M.H. Lee, D.J. Kim, J.S. Park, S.W. Kim, T.K. Song, M.H. Kim, W.J. Kim, D. Do and I.K. Jeong, High-performance lead-free piezoceramics with high Curie temperatures, *Adv. Mater.* **27**, 6976 (2015), https://doi.org/10.1002/adma. 201502424.

[17]Y. Zhao, J. Liu, X. Zhang and H. Zhou, Domain switching mechanism of orthorhombic-tetragonal coexistence (Li, K, Na)NbO_3 ceramics, *J. Alloys Compd.* **763**, 695 (2018), doi:10.1016/j.jallcom.2018.06.005.

[18]J. Koruza, A.J. Bell, T. Frömling, K.G. Webber, K. Wang and J. Rödel, Requirements for the transfer of lead-free piezoceramics into application, *J. Materiomics* **4**, 13 (2018), doi:10.1016/j.jmat.2018.02.001.

[19]J. Wu, Y. Wang, D. Xiao, J. Zhu, P. Yu, L. Wu and W. Wu, Piezoelectric properties of $LiSbO_3$-modified $(K_{0.48}Na_{0.52})NbO_3$ lead-free ceramics, *Jpn. J. Appl. Phys.* **46**, 7375 (2007), doi:10.1143/JJAP.46.7375.

[20]G. Ray, N. Sinha and B. Kumar, Environment friendly novel piezoelectric 0.94$[Na_{0.8}K_{0.2}NbO_3]$-0.06$LiNbO_3$ ternary ceramic for high temperature dielectric and ferroelectric applications, *Mater. Chem. Phys.* **142**, 619 (2013), doi:10.1016/j.matchemphys.2013.08.006.

[21]N.V. Dergunova, L.A. Reznitchenko, V.P. Sakhnenko, O.N. Razumovskaya and G.A. Geguzina, On the possibility of isomorphic substitutions in ferroelectrics with the perovskite- and pseudoilmenite-type structure, *Ferroelectrics* **247**, 107 (2000), doi:10.1080/00150190008214947.

[22]J. Chen, N. Su, X.L. Zhu, X.Q. Liu, J.-X. Zhang and X.M. Chen, Electric-field-controlled magnetism due to field-induced transition of $Pna2_1$/R3c in $Bi_{1-x}Gd_xFeO_3$ ceramics, *J. Materiomics* **7**, 967 (2021), doi:10.1016/j.jmat.2021.03.006.

[23]S. Sundari and R. Dhanasekaran, Influence of transition metal ions on multiferroic properties of lead-free NBT-BT ceramics, *J. Adv. Dielect.* **9**, 1950045 (2019), doi:10.1142/S2010135X19500450.

[24]P. Kumari, R. Rai, S. Sharma and M.A. Valente, Dielectric, electrical conduction and magnetic properties of multiferroic $Bi_{0.8}Tb_{0.1}Ba_{0.1}Fe_{0.9}Ti_{0.1}O_3$ perovskite compound, *J. Adv. Dielect.* **7**, 1750034 (2017), doi:10.1142/S2010135X17500345.

[25]R. Pandey, U. Shankar, S.S. Meena and A.K. Singh, Stability of ferroelectric phases and magnetoelectric response in multiferroic (1-x)$Bi(Ni_{1/2}Ti_{1/2})O_3$-$PbTiO_3$/x$Ni_{0.6}Zn_{0.4}Fe_2O_4$ particulate composites, *Ceram. Int.* **45**, 23013 (2019), doi:10.1016/j.ceramint.2019.07.348.

[26]K.P. Andryushin, L.A. Shilkina, I.N. Andryushina, M.O. Moysa, D.I. Rudzki and L.A. Reznichenko, Crystal structure, polarization properties and reverse nonlinearity of solid solutions of the KNN-PZT system in a wide range of external influences, *Ceram. Int.* **47**, 138 (2021), doi:10.1016/j.ceramint.2020.08.117.

[27]A.Z. Szeremeta, I. Lazar, A. Molak, I. Gruszka, J. Koperski, A. Soszyński and D. Kajewski, Improved piezoelectric properties of $Pb(Zr_{0.70}Ti_{0.30})O_3$ ceramics doped with non-polar bismuth manganite, *Ceram. Int.* **45**, 18363 (2019), doi:10.1016/j.ceramint.2019.06.051.

[28]K. Andryushin, L. Shilkina, I. Andryushina, A. Nagaenko, M. Moysa, S. Dudkina and L. Reznichenko, Features of the structure and electrophysical properties of solid solutions of the system (1-x-y) $NaNbO_3$-xKNbO3y$Cd_{0.5}NbO_3$, *Materials* **14**, 4009 (2021), doi:10.3390/ma14144009.

[29]K. Wang and J.-F. Li, Domain engineering of lead-free Li-modified (K,Na)NbO3 polycrystals with highly enhanced piezoelectricity, *Adv. Funct. Mater.* **20**, 1924 (2010), doi:10.1002/adfm.201000284.

[30]J.E. García, J.D.S. Guerra, E.B. Arajo and R. Pérez, Domain wall contribution to dielectric and piezoelectric responses in 0.65$Pb(Mg_{1/3}Nb_{2/3})$-0.35$PbTiO_3$ ferroelectric ceramics, *J. Phys. D, Appl. Phys.* **42**, 115421 (2009), doi:10.1088/0022-3727/42/11/115421.

[31]E. G. Fesenko, *Perovskite Family and Ferroelectricity* (Atomizdat, Moscow, 1972), 248 pp. (in Russian).

[32]C.B. Sawyer and C.H. Tower, Rochelle salt as a dielectric, *Phys. Rev.* **35**, 269 (1930).

[33]Y. Xu, *Ferroelectric Materials and their Applications* (Elsevier, Amsterdam, 1991).

[34]G. Metrat, Theoretical determination of domain structure at transition from twinned phase: Application to the tetragonal-orthorhombic transition of $KNbO_3$, *Ferroelectrics* **26**, 801 (1980), doi:10.1080/00150198008008175.

[35]V. Topolov, *Heterogeneous Ferroelectric Solid Solutions: Phases and Domain States*, 2nd edn. (Springer International, Cham, 2018).

[36]J. Fousek and V. Janovec, The orientation of domain walls in twinned ferroelectric crystals, *J. Appl. Phys.* **40**, 135 (1969), doi:10.1063/1.1657018.

[37]M. Moysa, V. Topolov, K. Andryushin, A. Nagaenko, L. Shilkina, M. Il'ina, O. Osotova, S. Sahoo and L. Reznichenko, Links between volume fractions of non-180 degree domains of the tetragonal and monoclinic phases in 0.75$NaNbO_3$ – 0.15$KNbO_3$ – 0.10$CdNb2O_6$, *Mendeley Data* **1**, 1 (2022), doi:10.17632/ngnc4rj8jy.1.